Precise Finite Difference Analysis of Lorentz Force Acting on Metal Nanoparticle Irradiated with Light

Takashi Yamaguchi[1, *], Mizue Ebisawa[1], and Shinichiro Ohnuki[2]

Abstract—A finite difference method in the frequency domain is evaluated to clarify characteristics of the Lorentz force exerted on a metal nanoscale particle by light irradiation. Numerical results are compared with exact values obtained from Mie theory to show that applying a smoothing algorithm to the surface of a nanoparticle increases the accuracy of the simulation. Analysis of the Lorentz force exerted between two spheres aligned closely indicates that strong forces cause the spheres to attract each other at the plasmon resonant frequency. It was also noticed that application of the smoothing algorithm was indispensable in order to achieve the above result.

1. INTRODUCTION

Metal nanoparticles have a key role in the development of biosensors [1, 2] and color materials [3–5] owing to their unique optical characteristics, such as strong absorption and scattering, caused by localized surface plasmon resonance (LSPR) at certain wavelengths. The wavelength of LSPR is mainly determined by the shape of the particles, the type of the metal, and the refractive index of the medium surrounding the particles [6]. Thus, aggregation of the particles, which can be identified by an increase in the particle size, changes the resonant wavelength normally towards the longer wavelength end of the spectrum. In the case of biosensing, since target analytes, such as biomolecules attached on a particle's surface, combine with the particle, we can detect them via a shift in the resonant wavelength. For use of these particles as color materials, control of their aggregation state is important to realize an expected color. We confirmed experimentally that a dispersion liquid of silver nanoparticles changes its color gradually due to aggregation when LED light at the plasmon resonance frequency impinges. Approaches that induce aggregation of the particles can be roughly divided into two categories — chemical and non-chemical methods [7]. Our interest, in this study, is in a non-chemical approach that uses the Lorentz force generated by light irradiation behaving as a dominant attracting force between the particles positioned at some distance each other [8–10]. The Lorentz force is also crucial in fine manipulations of particles by light. Although light commonly pushes any object forward, but it is possible to induce backward and lateral forces under certain conditions of the light source and the medium of the particles [11–13].

The Lorentz force acting on a particle is derived from electromagnetic fields inside and at the surface of the particle [14]. Mie's theory gives us a rigorous solution when the particle is represented as spheres [13], but numerical simulations are needed to investigate the relation between the Lorentz force and aggregation for multiple particles of arbitrary sizes, shapes, materials, and locations. Several techniques have been reported to analyze electromagnetic fields and the Lorentz force under various geometric configurations in both the time and frequency domains. Fujii [15] reported the particle size

dependency of the Lorentz force exerted on a metal cluster, touching two spheres, using the finite-difference time-domain (FDTD) method. Shalin et al. [16] investigated the motion of a nanoparticle placed on a plasmonic V-groove waveguide and driven by a light beam performing the finite-element method (FEM). Xiao and Chan [17] analyzed optical forces in arbitrarily shaped two-dimensional cylinders by applying the boundary-element method [18] and described the effect of their surface roughness on force enhancement. Chaumet and Rahmani [19] formulated a method based on the coupled dipole to compute the optical forces and torques on an object that has an arbitrary shape, permittivity, and permeability. In this study, we considered the finite difference in frequency domain (FDFD) method, in which Maxwell's equations, expressed in the frequency domain, are spatially discretized by using the central difference method. There were two reasons for this. Firstly, we need to know about the intensity of the forces in a steady state, because the velocity of light is much faster than that of the motion of particles. Secondly, the cubic cells in Yee's algorithm are very convenient for dealing with analysis models in which objects continuously change their position and direction with time. The FDFD method takes little computational time to generate a mesh compared with other techniques using an unstructured mesh.

In this study, improvement of the accuracy of the FDFD simulation, by smoothing of the boundary between a particle and a surrounding medium, was confirmed through analyses of the Lorentz force acting on a sphere, which is obtained from a volume integral of electromagnetic fields, and whose exact solution can be obtained from Mie theory. The dependence of the Lorentz force on the incident wavelength showed that the force exerted on a particle, or two particles, was enhanced by electromagnetic fields at the wavelength of LSPR.

2. FDFD ALGORITHM FOR ANALYSIS OF LORENTZ FORCE

To treat an incident wave propagating in an arbitrary direction simplistically, we used Maxwell's equations expressed in the frequency domain, in which electromagnetic fields $(\boldsymbol{E}, \boldsymbol{H})$ are separated into incident $(\boldsymbol{E}^i, \boldsymbol{H}^i)$ and scattered $(\boldsymbol{E}^s, \boldsymbol{H}^s)$ fields [20] as follows:

$$\nabla \times \boldsymbol{E}^s(\boldsymbol{r}) + j\omega\mu(\boldsymbol{r})\boldsymbol{H}^s(\boldsymbol{r}) = j\omega\{\mu_{sr} - \mu(\boldsymbol{r})\}\boldsymbol{H}^i(\boldsymbol{r})$$
$$-\nabla \times \boldsymbol{H}^s(\boldsymbol{r}) + j\omega\varepsilon(\boldsymbol{r})\boldsymbol{E}^s(\boldsymbol{r}) = j\omega\{\varepsilon_{sr} - \varepsilon(\boldsymbol{r})\}\boldsymbol{E}^i(\boldsymbol{r}) \tag{1}$$

where ω is the angular frequency of the incident wave; μ and ε are the permeability and permittivity of the particle, respectively; μ_{sr} and ε_{sr} are those of the surrounding medium. In general, the value of ε for metal is a complex value in the visible light region. The time factor is given by $e^{j\omega t}$. The permeabilities, μ and μ_{sr}, were fixed at μ_0, the permeability of free space, throughout this paper. In Eq. (1), the incident fields, $\boldsymbol{E}^i$ and $\boldsymbol{H}^i$, are given values, as an initial condition of the simulation and the scattered fields, $\boldsymbol{E}^s$ and $\boldsymbol{H}^s$, are unknowns that we want to obtain. Discretizing Eq. (1) with the finite-difference approximation yields simultaneous linear equations, which can be solved by using various well-known numerical techniques, such as iterative or direct solvers.

The time-averaged Lorentz force $\boldsymbol{F}$ acting on each particle is calculated from a volume integral of Maxwell's stress tensors, $\tilde{\boldsymbol{T}}^e$ and $\tilde{\boldsymbol{T}}^m$, over the particle [14]:

$$\boldsymbol{F} = \frac{1}{2}\text{Re}\int_{V'}\left(\nabla \cdot \tilde{\boldsymbol{T}}^e + \nabla \cdot \tilde{\boldsymbol{T}}^m\right)dV \tag{2}$$

where

$$\tilde{\boldsymbol{T}}^e = \varepsilon_{sr}\begin{bmatrix} |E_x|^2 - |\boldsymbol{E}|/2 & E_x E_y^* & E_x E_z^* \\ E_y E_x^* & |E_y|^2 - |\boldsymbol{E}|/2 & E_y E_z^* \\ E_z E_x^* & E_z E_y^* & |E_z|^2 - |\boldsymbol{E}|/2 \end{bmatrix}$$
$$\tilde{\boldsymbol{T}}^m = \mu_{sr}\begin{bmatrix} |H_x|^2 - |\boldsymbol{H}|/2 & H_x H_y^* & H_x H_z^* \\ H_y H_x^* & |H_y|^2 - |\boldsymbol{H}|/2 & H_y H_z^* \\ H_z H_x^* & H_z H_y^* & |H_z|^2 - |\boldsymbol{H}|/2 \end{bmatrix} \tag{3}$$

The superscript $*$ denotes the complex conjugate. As Eq. (2) consists of just the optical constants of the surrounding medium and the total electromagnetic fields, we can compute the force $\boldsymbol{F}$ after an FDFD

simulation of electromagnetic fields is finished. The integral in Eq. (2) is implemented as a summation of the divergence of Maxwell's stress tensors at each cell in the analysis region, discretized spatially by using the finite-difference approximation. In Yee's cell, the electromagnetic fields are placed at the center of each node and surface, as usual, while all the components of the force are collocated together at the corners.

In the FDFD simulation, the surface of a spherical object, in this case the boundary between a particle and its surrounding medium, modelled with cubic cells, becomes stepwise, unfortunately. This poor modelling decreases the accuracy of the volume integral in Eq. (2), especially when the intensity of electromagnetic fields becomes large near the surfaces, as in plasmon resonance. To avoid this accuracy reduction, we applied a subpixel smoothing technique, which was developed for the FDTD method [21], to the FDFD method. Although this technique is applicable to both isotropic and anisotropic media [22], in this section we discuss isotropic complex permittivity considering the dispersibility of metals. The modified permittivity is defined by

$$\tilde{\varepsilon}(\boldsymbol{r}) = \left[\langle \varepsilon^{-1}(\boldsymbol{r}) \rangle \{ \boldsymbol{n}(\boldsymbol{r}) \otimes \boldsymbol{n}(\boldsymbol{r}) \} + \langle \varepsilon(\boldsymbol{r}) \rangle^{-1} \{ \boldsymbol{1} - \boldsymbol{n}(\boldsymbol{r}) \otimes \boldsymbol{n}(\boldsymbol{r}) \} \right]^{-1} \tag{4}$$

where $\langle \cdot \rangle$ denotes the average over the volume that encloses the field component in question and is equal to that of the cell; $\boldsymbol{n}$ is the vector normal to the boundary between the particle and the surrounding medium at each cell. The boundary was assumed flat in each cell, and we computed the average and the harmonic average of permittivity by dividing a cell into 1000 subcells. Applying this averaged permittivity allows to change continuously the particle size regardless of the cell size but blurs the surface of the particle and makes the integral range unclear in (2). In our simulation, if the center of a cell was inside the object, we added the cell into the integral range regardless of the value of the permittivity.

3. NUMERICAL RESULTS

We first analyzed the Lorentz force acting on a silver sphere of radius $a = 15\,\text{nm}$, in free space, for various wavelengths. In our experiment of color change, silver nanoparticles were dispersed in water. However, the resonant wavelength in both cases of free space and water is existed in the blue region and the color of the dispersion liquid redshifts by aggregation, thus we used the condition of free space to simplify the analysis model. The complex permittivity of silver was calculated from the Lorentz-Drude model [23, 24]. The spatial discrete intervals Δx, Δy, and Δz were each $1.5\,\text{nm}$. The incident field was a plane wave polarized in the y-direction and propagated in the positive z-direction. The un-split perfectly matched layers [25] of 10 cells enclosed the analysis region as an absorbing boundary condition. We implemented a FDFD code, in which the BiCGStab(l) method [26] was applied as an iterative solver, using the general-purpose computing on graphics processing units (GPGPU) technology in a manner similar to that of FDTD [20]. The order, l, of BiCGStab(l) was 7. Under this analysis condition, the Lorentz force, $\boldsymbol{F}$, is comprised of only the z-component, which corresponds to the direction in which
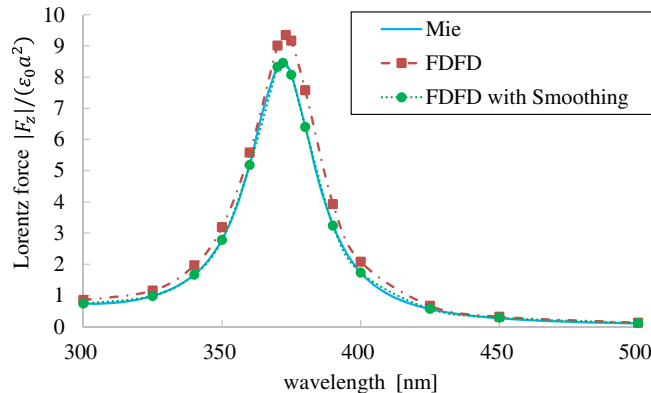

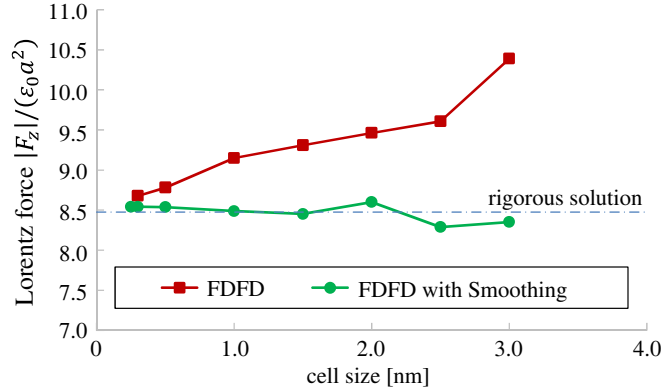**Figure 1.** Lorentz force acting on silver sphere against wavelength.

Figure 2. Cell size dependence of FDFD simulations.

the incident wave travels. Figure 1 shows the Lorentz force, F_z, normalized by $\varepsilon_0 a^2$ against incident wavelength, λ. As is shown, the Lorentz force was enhanced near $\lambda = 370\,$nm by LSPR in both the exact solution and the results of the FDFD simulations. The good agreement of the dotted line with the solid line within all the wavelength range indicates that the accuracy of the FDFD method was increased significantly by the effect of the smoothing technique. The norm of the relative error was reduced from 1.26×10^{-1} to 3.92×10^{-3}. In Figure 2, the FDFD results, both with and without the smoothing, are plotted versus cell size. The incident wavelength was fixed at $372\,$nm, the peak wavelength of the rigorous solution. All other conditions were the same as in the above simulation. From the dependence of cell size, the relative error, even at the $2.5\,$nm cell size, can be smaller than that of the standard FDFD at the $0.3\,$nm cell size when using the smoothing approach. Unlike scattered fields at a certain distance from the surface, the stairstep approximation of a curved face has a significant negative impact on the analysis of the Lorentz force. This improvement in accuracy would be quite effective when we analyze a large field in which several particles aggregate.

When two metal nanoparticles come within close proximity of each other, a strong attractive force is generated between them by interactions of LSPR. The FDFD method is a powerful way to deal with arbitrarily shaped particles, but here we considered simply a two sphere case to show clearly the difference from the single sphere case above. Figure 3 shows the comparison of the standard FDFD and the FDFD with the smoothing algorithm applied in the analysis of the normalized attractive force, $|F_y|/(\varepsilon_0 a^2)$, acting on the two silver spheres placed separately at a distance of $3\,$nm. The analysis conditions were the same as in the case of a single sphere. In this setup, the Lorentz force acts strongly in the y-direction, which corresponds with the polarization direction of the incident wave and the aligned direction of the objects. As is clear from Figure 3, the results of the two methods differed significantly more than in the case of a single sphere, thus the smoothing of boundaries must be applied when
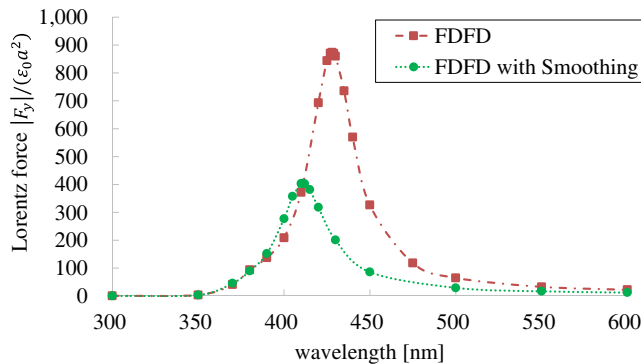

Figure 3. Attractive force generated between two spheres placed separately at distance of $3\,$nm.
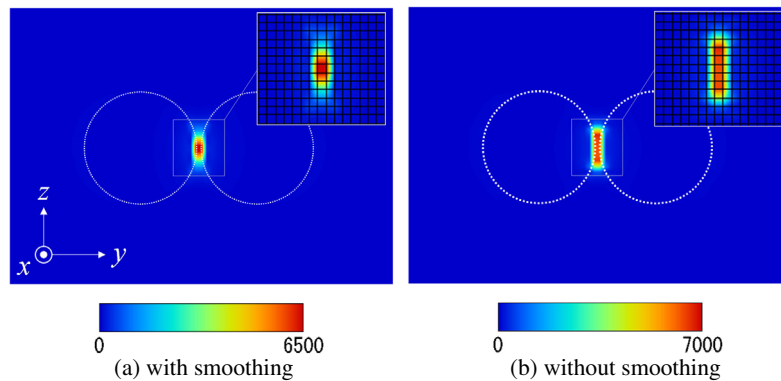
Figure 4. Distribution of the electric field intensity $|\boldsymbol{E}|^2$.

several particles aggregate. We confirmed that the characteristics computed by using FDFD applied the smoothing algorithm were stable independent from the cell size and can be considered as reference solutions. Figure 4 depicts the distribution of the electric field intensity, $|\boldsymbol{E}|^2$, on the y-z plane passing through the centers of the spheres. The incident wavelength was assumed to be the same as the resonant wavelength of each method. As is shown, large energy was confined between the particles in both cases, but its distribution in Figure 4(a) was narrower than that in Figure 4(b) because of the accurately modelled curved surface.

4. CONCLUSION

It was found that the Lorentz force acting on metal nanoparticles could be computed accurately by using the FDFD method with a subpixel smoothing technique. The numerical results showed that the Lorentz force was enhanced at the plasmon resonance frequency. When two spheres aggregated, the advantage of the smoothing was significantly increased.

REFERENCES

1. Anker, J. N., W. P. Hall, O. Lyandres, N. C. Shah, J. Zhao, and R. P. van Duyne, "Biosensing with plasmonic nanosensors," *Nat. Mater.*, Vol. 7, 442–453, 2008.

2. Guoa, L., J. A. Jackman, H. H. Yang, P. Chen, N. J. Cho, and D. H. Kim, "Strategies for enhancing the sensitivity of plasmonic nanosensors," *Nano Today*, Vol. 10, No. 2, 213–239, 2015.

3. Hsu, C. W., B. Zhen, W. Qiu, O. Shapira, B. G. DeLacy, J. D. Joannopoulos, and M. Solijačić, "Transparent displays enabled by resonant nanoparticle scattering," *Nat. Commun.*, Vol. 5, 2014.

4. Colomban, P., "The use of metal nanoparticles to produce yellow, red and iridescent colour, from Bronze Age to Present Times in lustre pottery and glass: Solid state chemistry, spectroscopy and nanostructure," *J. Nano Res.*, Vol. 8, 109–132, 2009.

5. Blosi, M., S. Albonetti, F. Gatti, G. Baldi, and M. Dondi, "Au-Ag nanoparticles as red pigment in ceramic inks for digital decoration," *Dyes Pigm.*, Vol. 94, 355–362, 2012.

6. Bohren, C. F. and D. R. Huffman, *Absorption and Scattering of Light by Small Particles*, Wiley-VCH, Weinheim, Germany, 2008.

7. Elimelech, M., X. Jia, J. Gregory, and R. Williams, *Particle Deposition and Aggregation: Measurement, Modelling and Simulation*, Butterworth-Heinemann, MA, USA, 1995.

8. Burns, M. M., J. M. Fournier, and J. A. Golovchenko, "Optical binding," *Phys. Rev. Lett.*, Vol. 63, No. 12, 1233–1236, 1989.

9. Kimura, K., "Photoinduced coagulation of Au nanocolloids," *J. Phys. Chem.*, Vol. 98, No. 8, 2143–2147, 1994.

10. Kimura, K., "Photoenhanced van der Waals attractive force of small metallic particles," *J. Phys. Chem.*, Vol. 98, No. 46, 11997–12002, 1994.

11. Chen, H., S. Liu, J. Zi, and Z. Lin, "Fano resonance-induced negative optical scattering force on plasmonic nanoparticles," *ACS Nano*, Vol. 9, No. 2, 1926–1935, 2015.

12. Chen, H., C. Liang, S. Liu, and Z. Lin, "Chirality sorting using two-wave-interference induced lateral optical force," *Phys. Rev. A*, Vol. 93, No. 5, 053833, 2016.

13. Chen, H., Y. Jiang, N. Wang, W. Lu, S. Liu, and Z. Lin, "Lateral optical force on paired chiral nanoparticles in linearly polarized plane waves," *Opt. Lett.*, Vol. 40, No. 23, 5530–5533, 2015.

14. Stratton, J. A., *Electromagnetic Theory*, McGraw-Hill, NY, USA, 1941.

15. Fujii, M., "Radius-dependent binding or repelling forces exerted on metal nano-sphere clusters by infrared-induced plasmonic resonance," *Opt. Commun.*, Vol. 285, No. 21–22, 4553–4557, 2012.

16. Shalin, A. S., P. Ginzburg, P. A. Belov, Y. S. Kivshar, and A. V. Zayats, "Nano-opto-mechanical effects in plasmonic waveguides," *Laser. Photon. Rev.*, Vol. 8, No. 1, 131–136, 2014.

17. Xiao, J. J. and C. T. Chan, "Calculation of the optical force on an infinite cylinder with arbitrary cross section by the boundary element method," *J. Opt. Soc. Am. B*, Vol. 25, No. 9, 1553–1561, 2008.

18. Sikora, J., M. Pańczyk, and P. Wieleba, "Hybrid boundary element method applied for diffusion tomography problems," *Computer Vision in Robotics and Industrial Applications*, World Scientific, 197–229, 2014.

19. Chaumet, P. C. and A. Rahmani, "Electromagnetic force and torque on magnetic and negative-index scatters," *Opt. Express*, Vol. 17, No. 4, 2224–2234, 2009.

20. Demir, V., "Graphics processor unit (GPU) acceleration of finite-difference frequency-domain (FDFD) method," *Progress In Electromagnetics Research M*, Vol. 23, 29–51, 2012.

21. Deinega, A. and I. Valuev, "Subpixel smoothing for conductive and dispersive media in the finite-difference time-domain method," *Opt. Lett.*, Vol. 32, No. 23, 3429–3431, 2007.

22. Kottke, C., A. Farjadpour, and S. G. Johnson, "Perturbation theory for anisotropic dielectric interfaces, and application to subpixel smoothing of discretized numerical methods," *Phys. Rev. E*, Vol. 77, 036611, 2008.

23. Rakić, A. D., A. B. Djurišić, J. M. Elazar, and M. L. Majewski, "Optical properties of metallic films for vertical-cavity optoelectronic devices," *Appl. Opt.*, Vol. 37, No. 22, 5271–5283, 1998.

24. Yamaguchi, T., "Finite-difference time-domain analysis of Hemi-Teardrop-shaped near-field optical probe," *Electron. Lett.*, Vol. 44, No. 4, 310–311, 2008.

25. Roden, J. A. and S. D. Gedney, "Convolutional PML (CPML): An efficient FDTD implementation of the CFS-PML for arbitrary media," *Microw. Opt. Technol. Lett.*, Vol. 27, No. 5, 334–339, 2000.

26. Sleijpen, G. L. G. and D. R. Fokkema, "BiCGstab(l) for linear equations involving unsymmetric matrices with complex spectrum," *ETNA*, Vol. 1, 11–32, 1993.